THE ASTROPHYSICAL JOURNAL, 286:509–516, 1984 November 15

EMISSION-LINE GAS ASSOCIATED WITH THE RADIO LOBES OF THE HIGH-LUMINOSITY RADIO SOURCE 3C 171

T. M. HECKMAN,[1,2,3,4] W. J. M. VAN BREUGEL,[3,4,5] AND G. K. MILEY[3,4,6]

Received 1984 January 24; accepted 1984 June 1

ABSTRACT

We report the discovery of spatially extended optical emission-line gas associated with the radio lobes of the high-redshift ($z = 0.2384$) radio galaxy 3C 171. This is the first known case of such an association in a high-luminosity ($L_{\rm radio} \sim 10^{44}$ ergs s^{-1}) radio source. The relationship of the gas and the radio source follows trends seen in radio sources of much lower luminosity. The emission-line gas occurs adjacent to (along the boundaries of) the bright regions of radio emission; the radio source morphology shows strong, abrupt "bends" in the vicinity of the emission-line gas; the radio emission is probably Faraday depolarized at locations of overlap between the emission-line gas and the radio plasma; the emission-line region is relatively small ($\sim$50 kpc); the gas velocities range up to almost 10^3 km s^{-1}; the emission-line spectrum of the gas associated with the radio lobes bears a strong spectroscopic resemblance to gas in the narrow-line region of active nuclei.

3C 171 is noteworthy in several respects. First, 3C 171 demonstrates that highly luminous radio sources and outer hot spot–dominated Fanaroff-Riley class II sources are capable of entraining significant amounts of cool, dense (optically detectable) material into their boundary layers. Second, the high luminosity of 3C 171 and the modest emission-line velocities observed place very severe energetic constraints on models in which the emission-line gas is comoving with the energy-carrying jet fluid (mass flow rates in excess of $10^3\ M_\odot$ yr^{-1} would be implied). The strongly asymmetric velocity field seen in the emission-line gas (a change of 600 km s^{-1} to the west of the nucleus compared with $\lesssim$50 km s^{-1} to the east) probably provides additional evidence against the gas being comoving jet material. Third, the size of the gas velocities observed and the strongly asymmetric velocity field imply that the gas is not simply quiescent material in the halo of a galaxy. Instead, the radio source is having a dynamically significant impact. Finally, the faint blue continuum we detect near the radio lobes may represent evidence for a local photoionization source for the emission-line gas. Collisional ionization by shocks is ruled out by the low observed gas temperatures ($\leq 2 \times 10^4$ K).

Subject headings: galaxies: individual — radio sources: extended — radio sources: galaxies

I. INTRODUCTION

There are now more than half a dozen cases known in which optical emission-line gas is associated with the radio lobes, or jets, of an extragalactic radio source. The properties of these objects have been reviewed recently by van Breugel and Heckman (1982) and Miley (1983).

Some of the most interesting questions regarding the associated regions of emission-line gas and radio plasma are:

1. What is the origin of the emission-line gas: entrained circumnuclear material (De Young 1981, 1982), compressed and shocked ambient clouds, or thermally unstable jet material (Hardee, Eilek, and Owen 1980)?

2. Do the emission-line velocities represent either the flow velocities of the energy-carrying jet fluid or the outward translational velocities of the radio hot spots?

3. What is the relationship between the presence of emission-line gas and the properties of the radio source itself (i.e., why do some radio sources have associated line-emitting gas)?

4. By what mechanism is the emission-line gas kept visible (at $T \gtrsim 10^4$ K)?

We report here the detection of optical emission-line gas associated with the radio lobes of 3C 171 (identified with an N galaxy at $z = 0.2384$). The global properties of 3C 171 are listed in Table 1. These new data are interesting in that they extend our study of such associations to a radio source an order-of-magnitude more powerful than the most radio-luminous such case previously known (3C 277.3 = Coma A; Miley *et al.* 1981; van Breugel *et al.* 1984). This allows us to progress closer to answers to the questions posed above.

TABLE 1

GLOBAL PROPERTIES OF 3C 171

Optical[a]	
Redshift	0.2384
Linear/angular size ratio	3.4 kpc arcsec^{-1}
Galaxy type	N
m_v	18.9
H_0 (assumed)	75 km s^{-1} Mpc^{-1}
q_0 ($''$)	0
Radio[b]	
Flux density (1400 MHz)	3.8 Jy
Total radio luminosity (10^7–10^{11} Hz)	10^{44} ergs s^{-1}
Spectral index ($S \sim \nu^{-\alpha}$)	0.94

[a] Burbidge and Crowne 1979.
[b] Kühr *et al.* 1979.

[1] Astronomy Program, University of Maryland.
[2] Alfred P. Sloan Foundation Fellow.
[3] Visiting Observer at the Kitt Peak National Observatory of the National Optical Astronomy Observatories, operated by AURA, Inc., under contract to the National Science Foundation.
[4] Visiting Observer at the National Radio Astronomy Observatory, operated by AUI, under contract to the National Science Foundation.
[5] Department of Astronomy, University of California, Berkeley.
[6] Sterrewacht Leiden.

TABLE 2

OBSERVING PARAMETERS

PARAMETER	VLA (Imaging and Polarimetry)			4 METER MAYALL		
				Prime Focus CCD (Imaging)	HGVS (Spectroscopy)	Cryogenic Camera (Spectroscopy)
Wavelength(s)	2 cm	6 cm	20 cm	R	5110–5800 Å	4560–7890 Å
Spatial resolution	0.″11	0.″35	1.″1	1″	3″	2″
Velocity resolution	...	...	...	...	200 km s^{-1}	700 km s^{-1}
Position angles	...	...	...	...	95°	12°; 45°; 102°
Date		1983 Oct		1982 Jan	1982 Apr	1982 Dec; 1983 Dec

II. OBSERVATIONS

a) *Optical*

Our optical observations of 3C 171 consist of two sets of long-slit optical spectroscopic data, and one set of imaging data, all taken with the 4 m Mayall telescope at the Kitt Peak National Observatory (see Table 2).

1. In 1982 April we observed 3C 171 with the High-Gain Video Spectrometer (HGVS). The 2″ wide spectrograph slit was oriented approximately along the radio axis of 3C 171 (P.A. = 95°). Redshifted [O III] $\lambda\lambda$5007, 4959 and Hβ emission lines were observed with $\sim$200 km s^{-1} spectral and $\sim$3″ spatial resolution. Standard procedures were followed in the acquisition, calibration, and analysis of these data (see, e.g., Heckman *et al.* 1982).

2. In 1982 December and 1983 December we observed 3C 171 with the Cryogenic Camera (CCD spectrograph). Data were obtained along (P.A. = 102°) and orthogonal to (P.A. = 12°) the radio axis and at an intermediate position (P.A. = 45°) with a 2.″5 wide slit. These data have $\sim$700 km s^{-1} spectral and $\sim$2″ spatial resolution, which represent lower velocity resolution but better spatial resolution and considerably higher signal-to-noise ratio than the HGVS data. For a description of the Cryogenic Camera and the procedures followed see Balick and Heckman (1983). Some of our Cryogenic Camera data in P.A. = 102° are shown in Figure 1 (Plate 18).

3. In 1982 January we obtained a broad-band (R) image of 3C 171 using the Prime Focus CCD under excellent observing conditions (seeing $\sim$1″). For details see van Breugel *et al.* (1984). We display a portion of our CCD image in Figure 2 (Plate 19).

b) *Radio*

We have observed 3C 171 with the NRAO Very Large Array (VLA) in the standard A configuration at 2 cm (14,965 MHz), 6 cm (4885 MHz), and 20 cm (1465 MHz) during 1983 October. The source 0642+449 was used as the phase calibrator, 3C 286 was used as the primary flux and absolute polarization position angle calibrator, and 3C 84 was used as the instrumental polarization calibrator. The visibility data at all three wavelengths were calibrated using the standard VLA DEC-10 programs. Maps were produced, CLEANed, and self-calibrated using the standard AIPS programs on the VLA VAX 11-780. Various details concerning the observations and final maps are listed in Table 2.

III. RESULTS

a) *Radio Maps*

i) *Morphology*

The remarkable radio morphology of 3C 171 at 2, 6, and 20 cm is illustrated in Figure 3.

1. A central component is detected at 2 cm (4.2 $\pm$ 0.5 mJy) and at 6 cm (2.0 $\pm$ 0.4 mJy). Since this component is unresolved (<0.″05 at 2 cm) and has an inverted spectrum, it can be identified with the active nucleus itself.

2. Straddling the nuclear source in P.A. $\sim$102° are two very bright compact radio hot spots (4.″4 E and 4.″7 W), whose structure can be most clearly discerned in the 2 cm map (Figs. 3*a*, 3*b*). Both components are resolved in this map and are several hundred pc in size (see Table 3).[7] The W hot spot (Fig. 3*b*) is elongated toward the N, perpendicular to the radio axis. The E hot spot is elongated along the radio axis.

3. The 6 cm map (Fig. 3*c*) shows that the two hot spots are embedded in regions of more diffuse emission $\sim$3″ ($\sim$10 kpc) in size (the radio lobes). Both lobes have triangular morphologies with peculiarly flat outer edges. However, while the E lobe is fairly symmetric with respect to the radio axis, the W lobe is strongly asymmetric to the north (toward the diffuse radio plume discussed below and in the same sense as the W hot spot discussed above).

4. The 20 cm map (Fig. 3*d*) best illustrates the faint, large-scale plumes of radio emission associated with both radio lobes. To the W, the radio emission (NW plume) stretches some 22″ (74 kpc) to the N of the W hot spot. A brightness enhancement is seen at the end of this plume. The large-scale structure of the E half of the source is much more symmetric,

[7] We take $H_0 = 75$ km s^{-1} Mpc^{-1} and $q_0 = 0$ throughout this paper.

TABLE 3

MINIMUM ENERGY PARAMETERS FOR THE RADIO SOURCE

Component	Size (arcsec)	Position Angle (degrees)	Magnetic Field (gauss)	Pressure (K cm^{-3})	Total Energy (ergs)
W hot spot	0.06 × 0.14	8	7.4×10^{-4}	1.6×10^{8}	4.7×10^{55}
E hot spot	0.11 × 0.29	119	5.0×10^{-4}	7.2×10^{7}	5.1×10^{55}
NW plume	5 × 22	346	1.7×10^{-5}	8.2×10^{4}	5×10^{57}
NE plume	6 × 12	7	1.7×10^{-5}	8.2×10^{4}	1×10^{58}
SE plume	4 × 7	165			

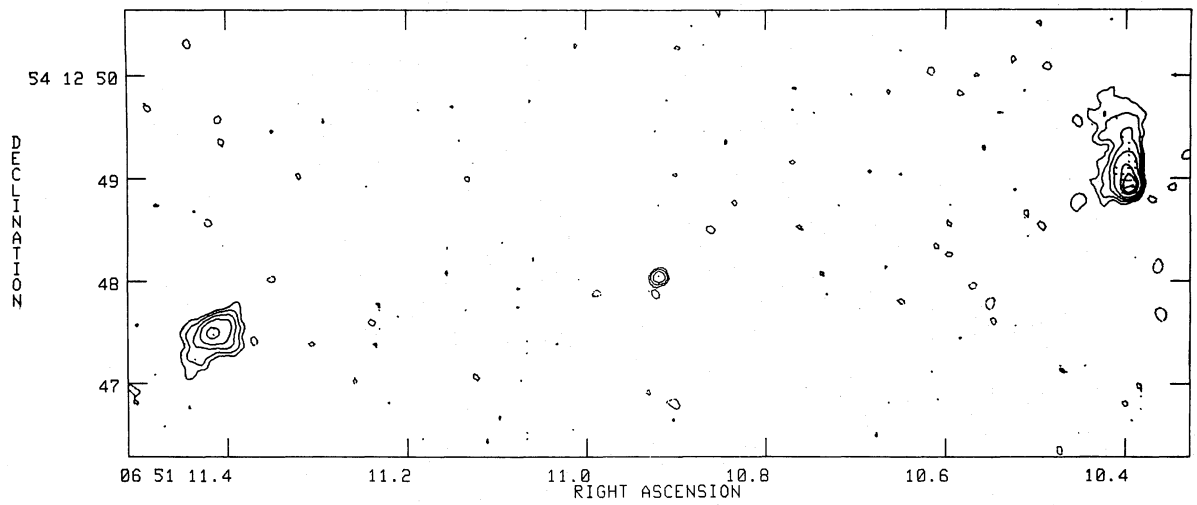

FIG. 3*a*

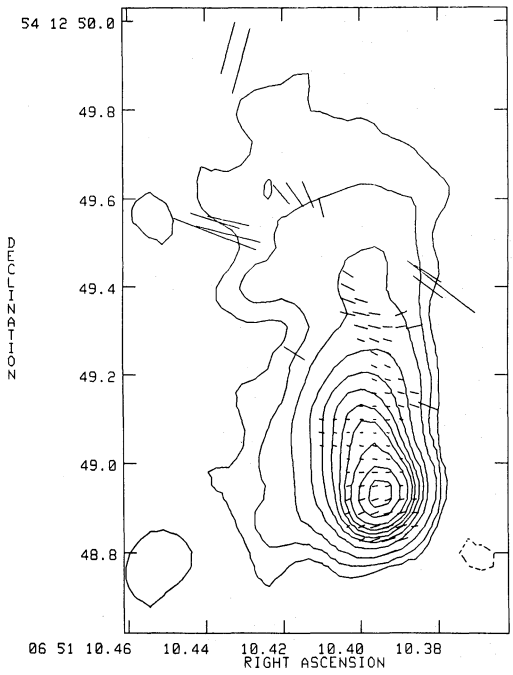

FIG. 3*b*

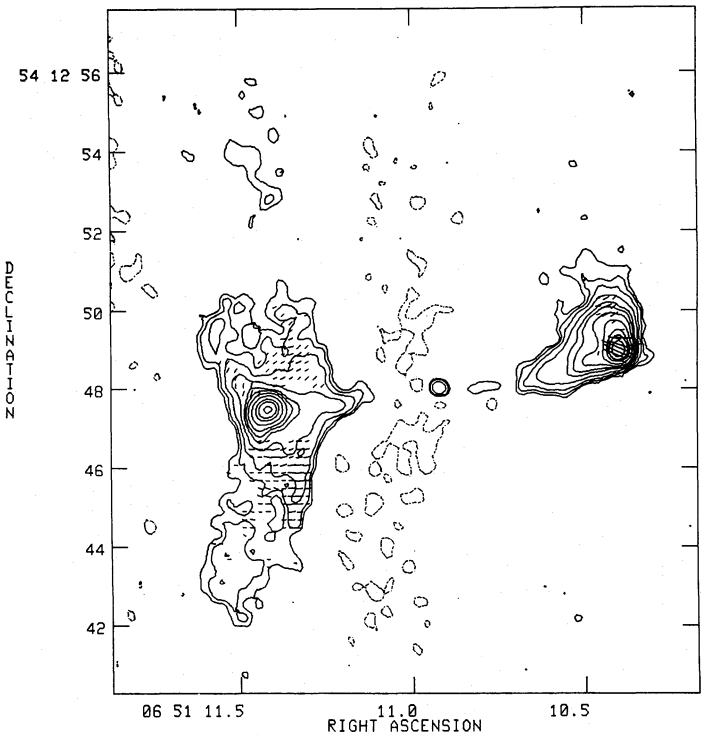

FIG. 3*c*

FIG. 3.—Contour plots of the VLA maps of 3C 171 at three wavelengths. (*a*) Map of the total intensity at 2 cm (0″.11 resolution). The contour levels are at −0.5, 0.5, 1.0, 2.0, 4.0, 10.0, and 15.0 mJy per beam. The lengths of the *electric* field vectors (no correction for Faraday rotation) are proportional to the linear polarized intensity with a scale 1″ = 47.6 mJy per beam. (*b*) Details of the 2 cm map of the W radio hot spot. The contour levels are at −0.5, 0.5, 1.0, 2.0, 4.0, 6.0, 8.0, 10.0, 12.0, 15.0, 20.0, and 25.0 mJy per beam. The electric field vectors have lengths proportional to the percent polarization with a scale 1″ = 959%. (*c*) The 6 cm total intensity map (0″.35 resolution), with contour levels of −0.4, 0.4, 0.6, 1.0, 2.0, 4.0, 6.0, 10.0, 20.0, 40.0, 60.0, and 100 mJy per beam. The electric field (polarized intensity) vectors have a scale of 1″ = 4.8 mJy per beam. (*d*) The 20 cm total intensity map (1″.1 resolution), with contour levels of −1.0, 1.0, 2.0, 3.0, 5.0, 10.0, 20.0, 30.0, 50.0, 100.0, 250.0, 500.0, and 1000.0 mJy per beam. The electric field vectors have a scale of 1″ = 6.8 mJy per beam.

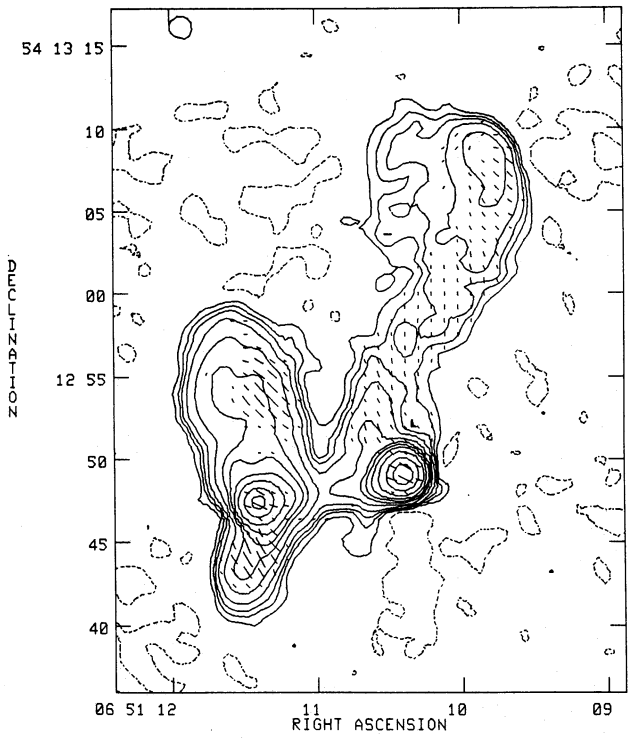

FIG. 3*d*

with plumes extending ~10″ both N and S (the NE and SE plumes). We emphasize that the difference between the E and W halves of the source is seen on all scales (hot spots, lobes, plumes), spanning a factor $\gtrsim 100$ in size. Note that this asymmetric plume morphology is not consistent with Laing's (1981) tentative suggestion that 3C 171 is a wide-angle tail source.

5. Despite the morphological peculiarities of 3C 171, we concur with its classification by Laing, Riley, and Longair (1983) as a Fanaroff-Riley (1974) class II (dominant outer hot spots) radio source.

ii) *Minimum-Energy Parameters*

We have calculated (Table 3) the pressures, magnetic field strengths, and total energies for the various radio components in 3C 171 assuming standard minimum energy conditions (cf. Miley 1980): namely, a filling factor of unity for the synchrotron-emitting plasma, equal relativistic electron and proton energies, and cylindrical forms for the radio components (for all components except for the NW plume the symmetry axis of the cylinder was taken to lie along the radio source axis in P.A. = 102°).

The derived values for these various parameters are typical for powerful extragalactic radio sources. However, the pressures in the two hot spots ($nT \sim 10^8$ K cm^{-3}) exceed by about an order of magnitude the highest pressures found in other radio sources with clearly associated optical emission-line gas (Heckman *et al.* 1982; van Breugel *et al.* 1984).

iii) *Polarization*

Since we have not mapped 3C 171 with comparable angular resolution at all three wavelengths, a detailed multifrequency comparison of the polarimetric properties of 3C 171 is not warranted. Nevertheless, several interesting conclusions can be drawn from our more limited data;

1. The percent polarization in and near the W hot spot decreases rapidly with wavelength: 10%–20% at 2 cm, 2%–3% at 6 cm, and 0.8% at 20 cm. The polarization vectors are nearly constant in direction throughout this region at 2 cm (Fig. 3*b*), so beam depolarization is unlikely to be responsible for the observed effect. Faraday depolarization is a much more plausible possibility.

2. No polarized flux is detected from the E hot spot at either 2 cm ($\leq 5\%$ polarized) or 6 cm ($\leq 0.4\%$ polarized). While some polarized flux is detected at 20 cm from the vicinity of the E hot spot (at the 1% level), it is likely that much of this is foreground/background diffuse polarized emission associated with the highly polarized NE and/or SE plumes (see below). Such polarized emission would be resolved out at 2 cm and 6 cm. Thus, the E hot spot may be even more strongly Faraday depolarized than its western counterpart.

3. The percent polarization at both 6 cm and 20 cm rises as a function of distance away from the inferred radio axis in both the E and W lobes. The 6 cm values climb to $\gtrsim 50\%$ at locations 1″–2″ N and S of the E hot spot and to ~15%–30% ~ 1″–2″ N of the W hot spot (see Fig. 3*b*). In contrast, the 6 cm percentage polarization remains $\lesssim 15\%$ 1″–2″ E of the W hot spot and $\lesssim 10\%$ 1″–2″ W of the E hot spot. At 20 cm, the increase is less abrupt; however, the percent polarization rises to values of ~35% at 7″ N and 3″ S of the E lobe and at 3″ N of the W lobe. The percent polarization remains high throughout the NW plume (~50% near the middle section of the plume and ~20% at its N termination).

4. Correcting the data for a rotation measure of $+53 \pm 2$ radians m^{-2} (Simard-Normandin, Kronberg, and Button 1981), the projected magnetic field lies along the long axes of the radio plumes. In the NW region this field geometry can be traced down to the small scale of the compact W hot spot at 2 cm.

b) Optical Imaging

From the data represented in the *R* band CCD image (Fig. 2) we can draw the following conclusions:

1. As imaged in the redshifted lines of Hβ and [O III] $\lambda\lambda$4959, 5007 (which are transmitted by the *R* filter), the extended emission-line gas has a complex morphology which is clearly related to that of the radio source. A curved filament extends ~5″ (~17 kpc) to the E of the nucleus. A relatively bright part of this filament runs for ~2″–3″ in P.A. ~15° at a distance ~3.″5–4″ E of the nucleus. This feature would lie parallel to, but inside, the flattened E boundary of the radio source (Fig. 3). The emission between this feature and the nucleus would lie along the inner S boundary of the E radio lobe. The emission to the W of the nucleus is centered on a knot ~3″ from the nucleus, with fainter emission extending out an additional 2″–3″. The brightest emission to the W would then lie between the nucleus and W radio lobe, but fainter emission would extend beyond the radio lobe. An additional knot of emission-line gas is located ~2.″5 SW of the nucleus, below the western region of radio emission. The overall detectable E/W extent of the gas is ~40 kpc, in rough agreement with the more sensitive spectroscopic data discussed below.

2. About 10 faint objects, some of which are nonstellar, are located within ~40″ (135 kpc) of 3C 171. Calibrating the *R* band fluxes from these objects relative to the known *R* band flux from 3C 171 itself (Yee and Oke 1978) implies that these objects would have $M_v \sim -19$ to -20 if they are at the same distance as 3C 171. This compares with Miller's (1981) estimate

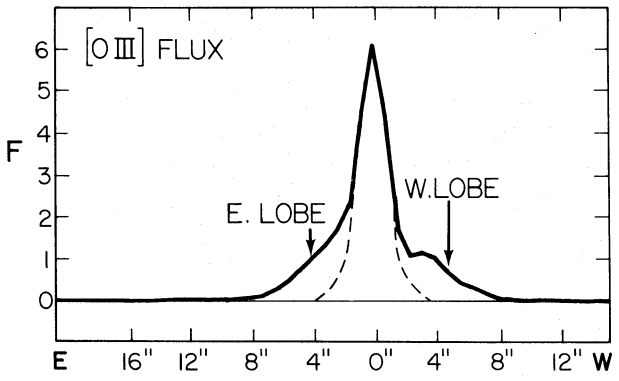

FIG. 4.—Plots of the [O III] λ5007 relative flux (in arbitrary units) as a function of position along the slit in P.A. = 102° (*solid line*) and P.A. = 12° (*dashed line*). Positions are given relative to the nucleus (1″ = 3.4 kpc), and the positions of the two radio lobes along P.A. = 102° are indicated.

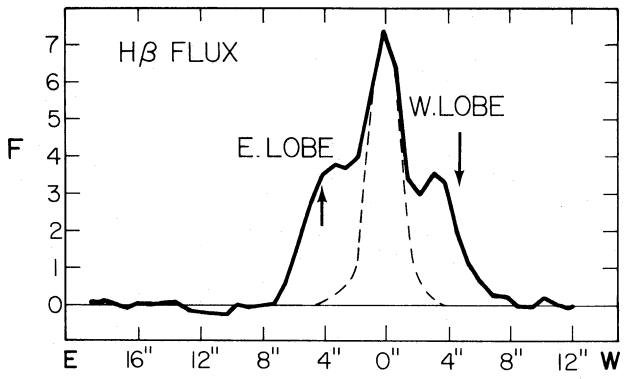

FIG. 5.—Same as Fig. 4, except for the Hβ line. Note the greater relative strength of Hβ in the extranuclear regions compared with [O III] in Fig. 4.

that the underlying galaxy (starlight only) in 3C 171 has $M_v \approx -20.4$, some 2 mag fainter than a first-ranked giant elliptical galaxy. At best then, 3C 171 is the brightest member of a group of galaxies but cannot be in a rich cluster. Thus, both the detailed radio morphology (see above) and the environment are at odds with an interpretation of 3C 171 as a wide-angle tail source (e.g., Owen and Rudnick 1976).

c) *Optical Spectroscopy*

i) *Spatial Distribution of the Gas*

In Figures 4 and 5 we show plots of the [O III] λ5007 and Hβ emission-line intensities, respectively, as a function of position along P.A. = 102° and 12°. The locations along P.A. = 102° of the two radio lobes are indicated in these figures as well. We have assumed spatial coincidence between the radio core (Fig. 3*a*) and the peak of the emission-line and continuum intensities in our data. These figures are clearly consistent with our imaging data (Fig. 2) and allow us to trace the gas over a region ~50 kpc across.

ii) *Kinematics of the Gas*

The run of the gas velocity along the radio axis is shown in Figure 6 (we consider the gas to be essentially unresolved spatially in the perpendicular direction). Line widths along the radio axis are shown in Figure 7. In both figures, the Cryogenic Camera CCD data (*dashed line*) are superior in quality, and inferences are drawn primarily from these data. From these figures, note the following:

1. The kinematics are not symmetric on the two sides of the nucleus. Velocities increase sharply by ~600 km s^{-1} ~ 3″ W of the nucleus, but remain within ~50 km s^{-1} of the nuclear velocity to the E. Farther to the W (~4″–6″), the velocities drop to +400 km s^{-1} relative to the nucleus. The knot 2″.5 SW of the nucleus is redshifted by ~150–200 km s^{-1} relative to the nucleus.

2. The very broad (FWHM ~ 800–1000 km s^{-1}) lines ~ 2″–3″ (7–10 kpc) to the W of the nucleus are probably the consequence of a blending by the seeing of the nuclear and the western high-velocity emission lines (compare Figs. 6 and 7). This is more apparent in the Cryogenic Camera data (higher spatial resolution). Elsewhere, the lines are ~500–600 km s^{-1} wide.

iii) *Emission-Line Spectra*

The emission-line spectra at three positions (the nucleus, and the E and W radio lobes) are displayed in Figure 8. We have

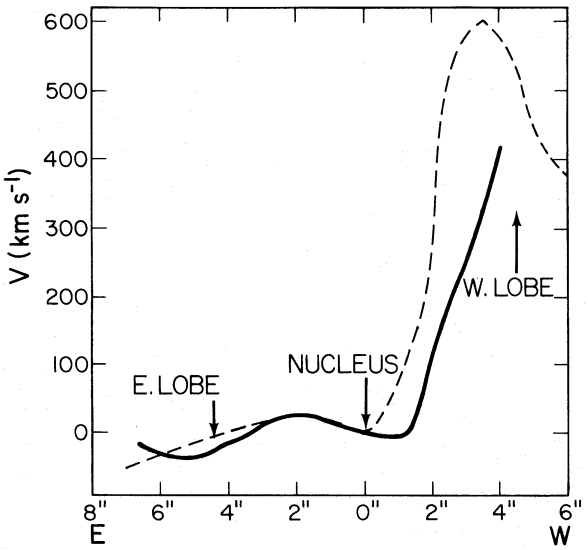

FIG. 6.—Gas velocity (from the [O III] λ5007 line) as a function of position along the slit in P.A. = 102° (Cryogenic Camera CCD data, *dashed line*) and P.A. = 95° (HGVS data, *solid line*). The positions of the nucleus and the two radio lobes are indicated. The Cryogenic Camera data, having higher signal-to-noise ratio and obtained under conditions of better seeing, are the more reliable (uncertainties ≲100 km s^{-1}).

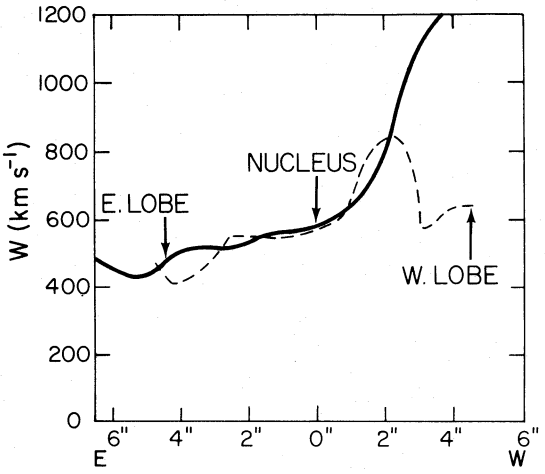

FIG. 7.—The full width at half-maximum of the [O III] λ5007 line (corrected for instrumental broadening) as a function of position along the slit. Widths are uncertain by ~100–200 km s^{-1}. Otherwise, the figure is as Fig. 6.

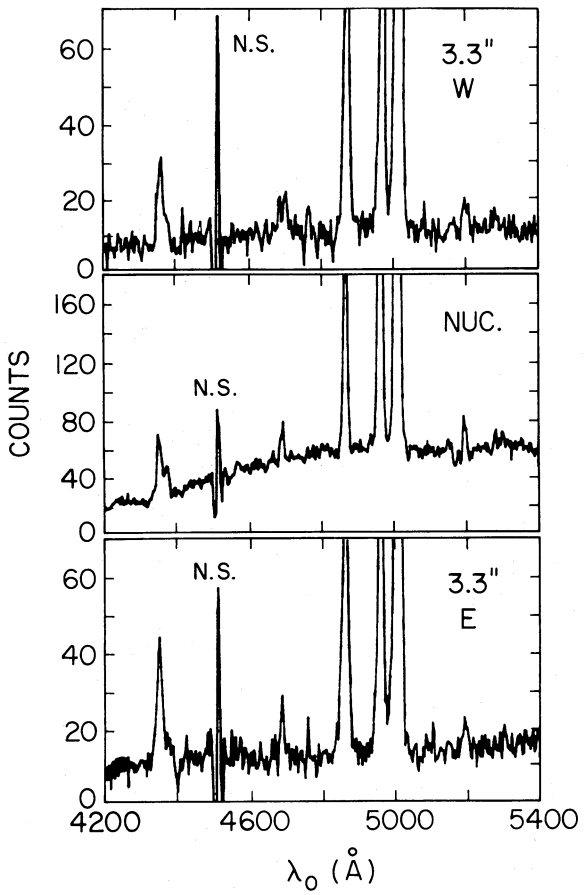

FIG. 8.—Plots of the CCD spectra (total counts in arbitrary units vs. wavelength in the 3C 171 rest frame). The three plots refer to regions 2".5 × 2".5 in extent centered on the nucleus (*middle plot*), 3".3 W (*top plot*), and 3".3 E (*bottom plot*).

used spectrophotometric data on the nucleus of 3C 171 (Miller 1981; Yee and Oke 1978; Keel and Miller 1983) to roughly calibrate our off-nuclear Cryogenic Camera data in terms of relative intensity. The results of this procedure are listed in Table 4.

The available data on 3C 171 then imply the following:

1. No broad wings can be discerned on Hβ in the nucleus. Thus, 3C 171 would be spectroscopically classified as a narrow-line radio galaxy. The overall nuclear spectrum agrees well with the spectra of other such objects (e.g., Koski 1978).

2. The degree of excitation ([O III] λ5007–to–Hβ) declines off-nucleus by a factor $\sim$2 (see also Figs. 4 and 5). In fact, the [O III]/Hβ ratio in the emission-line gas associated with the radio lobes resembles that of a Liner (low-ionization nuclear emission-line region) as defined by Heckman (1980). Such a spectrum is not unusual for gas associated with radio lobes (e.g., Heckman *et al.* 1982; van Breugel *et al.* 1984; van Breugel, Heckman, and Miley 1984*a*).

3. Miller's (1981) data yield an intensity ratio for [O III] (λ5007 + λ4959)/λ4363 of 63 in the nucleus, implying $T_e \sim$ 16,000 K there (Osterbrock 1974). [O III] λ4363 is only marginally detected in the radio lobes, giving $T_e \lesssim$ 20,000 K.

4. The data of Keel and Miller (1983) imply negligible dust-reddening in the nucleus, and our data then yield a similar result for the gas associated with the radio lobes.

TABLE 4

RELATIVE EMISSION-LINE FLUXES IN 3C 171

Line[a]	Nucleus[b]	3".3 E[c]	3".3 W[c]
[N I] λ5198	15	8	10
[O III] λ5007	670	325	290
Hβ	$\equiv$100	$\equiv$100	$\equiv$100
He II λ4686	16	18	13
[O III] λ4363	14	$\lesssim$10	$\lesssim$10
Hγ	51	60	54

[a] The total emission-line luminosity is estimated to be log $L_{\rm Lines} \sim 43.7 \pm 0.3$ in ergs s^{-1} for $H_0 = 75$ km s^{-1} Mpc^{-1}, and $q_0 = 0$.

[b] From Miller 1981 and W. Keel and J. S. Miller, private communication.

[c] The uncertainty due to noise is $\sim \pm 5$ units. Systematic errors between the blue and red ends of the off-nucleus spectra are likely to be larger. These regions are 2".5 × 2".5 in size centered 3".3 on either side of the nucleus in P.A. = 102° (see text).

5. The spectrophotometric data of Yee and Oke (1978) taken through a 5" aperture give $L_{[\rm O\ III]\ \lambda5007} \sim 3.5 \times 10^{42}$ ergs s^{-1}. Taking [O III]/H$\beta \sim 7$ on the nucleus, correcting for the spatially extended gas missed by the aperture, and assuming a typical case B hydrogen spectrum then implies a total emission-line luminosity of 5×10^{43} ergs s^{-1} (within a factor of 2). The gas associated with the radio lobes would account for about half this. Thus, $L_{\rm gas} \sim L_{\rm radio} \sim L_{\rm nucleus}$ (see immediately below).

iv) *The Optical Continuum*

Combining our Cryogenic Camera data with the spectrophotometric data of Yee and Oke (1978) and Miller (1981), we find:

1. A stellar continuum evidently contributes $\sim$50%–75% of the flux in a 5" (17 kpc) aperture centered on the nucleus. We detect the Mg I λ5174 stellar absorption line within $\sim$2" of the nucleus along both position angles.

2. The luminosity of the *nonstellar* optical/ultraviolet continuum computed by Yee and Oke is $\sim 3 \times 10^{43}$ ergs s^{-1}. Such a continuum extrapolated beyond the Lyman limit may be adequate to photoionize the emission-line gas (nuclear and extranuclear).

3. There is an excess blue continuum in the vicinity of the radio hot spots. This can be seen in Figure 9, in which we compare the radial falloff in the surface brightness of the blue and red continua in position angles along and perpendicular to the radio axis (from our Cryogenic Camera data). The broad-band image data (Fig. 2) is strongly contaminated by redshifted Hβ and [O III] $\lambda\lambda$4959, 5007 emission and cannot be used to confirm this result. Our spectroscopic data are too noisy to ascertain the nature of this blue continuum (i.e., young stars or nonthermal).

IV. DISCUSSION AND SUMMARY

We will structure our discussion by comparing and contrasting the properties of 3C 171 with those of other radio sources with associated regions of optical emission-line gas. In particular, we will emphasize why the discovery of such gas in a high-luminosity radio source is potentially important. The properties of associated radio/optical emission regions in radio sources have been summarized by van Breugel and Heckman (1982):

1. *The emission-line gas is brightest near (but slightly offset from) bright radio knots.* This is true of the gas in 3C 171 (see

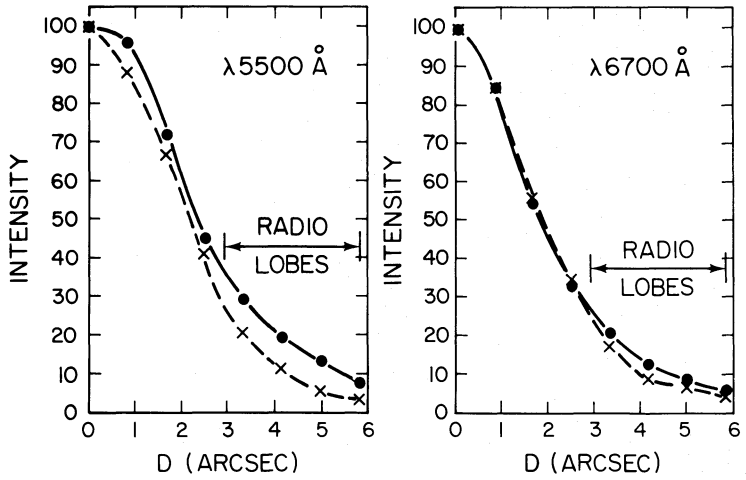

FIG. 9.—The continuum intensity in our Cryogenic Camera data as a function of distance from the nucleus along the radio axis in P.A. = 102° (*dots and solid lines*) and perpendicular to the radio axis in P.A. = 12° (*crosses and dashed line*). The left figure refers to the continuum at 5500 Å, while the right refers to 6700 Å (both in Earth's frame). In both figures, the nuclear continuum intensity has been arbitrarily scaled to 100 units, since our data are not well calibrated spectrophotometrically.

Fig. 5, for example). The fact that there is a rough morphological similarity between the bright optical and radio emission almost surely means that the radio source is responsible for "lighting up" the emission-line gas clouds. 3C 171 is particularly interesting in this sense since we have detected a faint blue continuum in the vicinity of the radio lobes and the brightest extranuclear gas. This continuum may represent the optical counterpart of an ionizing (synchrotron?) continuum produced locally in the radio hot spots or lobes.

The preferential occurrence of emission-line gas along the *boundaries* of the radio source is most plausibly interpreted as indicating that the gas is not nuclear ejecta, but is instead extranuclear material which has been mixed into the turbulent boundary layer ("cocoon") of the radio source (De Young 1981, 1982; Norman *et al.* 1982). De Young in fact suggested that sources having a Fanaroff and Riley (1974) class I morphology ("billowy", edge-darkened appearance) would be adept at this entrainment process because (he argued) the radio jets in these sources are subsonic or transonic and highly turbulent. 3C 171 is then important because it has an outer hot spot–dominated Class II morphology: such a morphology evidently does not preclude substantial entrainment. 3C 171 also demonstrates that highly radio-luminous sources (as well as the previously known low-luminosity sources with associated optical line emission) are capable of this entrainment process.

2. *The radio source structure is often strongly distorted, or bent, in the vicinity of the emission-line gas.* 3C 171 is perhaps the most spectacular example yet of this phenomenon. A sharp transition in the radio structure from an axis of 100° (the lobes/hot spots) to ~0° (the plumes) occurs in the region where the bright extranuclear emission-line knots are found. The distorted radio structure of 3C 171 is highly unusual and is not naturally explained by the standard mechanisms for distortion of a radio source since it is neither mirror nor inversion symmetric. What is rather remarkable is that the structure of 3C 171, while unusual, so closely resembles the structure of 3C 305 (Heckman *et al.* 1982), a much smaller radio source with associated emission-line gas. We do not propose a specific, detailed model for the distortion of 3C 171 but suggest (as we have done for other sources) that it is related to the propagation of light radio jets through a dense and highly inhomogeneous ambient medium.

3. *The radio source is strongly Faraday depolarized at locations where the optical emission-line gas overlaps the radio source.* Better data are needed to explore this in detail in 3C 171, but the basic phenomenon is evident. Since the gas is apparently located primarily in the outer layers of the radio source, and is highly clumpy, we propose that the radio emission is depolarized by an inhomogeneous "Faraday screen" of emission-line clouds (see van Breugel, Heckman, and Miley 1984*a* for a detailed elucidation of this model).

4. *The range of velocities in the gas is* $\lesssim 10^3$ km s^{-1}. In fact, the gas velocities seen in 3C 171 are the largest we have studied so far and are nearly as large as the most extreme velocities seen in a faint filament in Cen A (Graham 1983). The large velocities seen in cases like 3C 171 or Cen A are important because (even without allowing for projection effects) they are well in excess of velocities expected for quiescent (gravitationally bound) material in the outer halo of a galaxy. Thus, it is almost certain that the radio source is providing kinetic energy to the gas. The very large widths of the lines and the peculiarly asymmetric velocity field in 3C 171 provide additional evidence that the gas is in a highly perturbed state.

However, we believe that it is most unlikely that the emission-line gas is actually comoving with the energy-carrying material in the radio jets. 3C 171 provides very important evidence in this regard because of its high luminosity. In standard jet models (e.g., Bridle and Perley 1984), the jet energy is transported primarily in the form of the kinetic energy of a "cold" fluid. If the velocities seen in the gas in 3C 171 are representative of the velocity of the energy-carrying fluid, a mass flow rate of at least 1000 $M_\odot$ yr^{-1} is required, even if the jet energy is converted into radio synchrotron radiation with 100% efficiency. This seems highly implausible.

The strongly asymmetric velocity field in 3C 171 is also hard to account for naturally if the gas is comoving with the jet fluid (why does one jet appear to flow more than 10 times faster than the other even though the radio luminosities of the E and W lobes are nearly the same?). The radio source might be V-shaped, and (by chance) only one jet might lie nearly in the

plane of the sky. While such a projection effect cannot be ruled out as the cause of the kinematic asymmetry, we find this a rather artificial explanation. First, strong kinematic asymmetries are found in several other radio sources having far less distorted radio structures than 3C 171 (van Breugel *et al.* 1984; van Breugel, Heckman, and Miley 1984*b*). Second, there is no evidence that the *jets* are V-shaped: The two radio hot spots are almost exactly collinear with the nucleus. We note further that the emission-line gas is exclusively associated with this collinear portion of the radio source. Projection effects severe enough to produce an apparent kinematic asymmetry with an amplitude exceeding 10 while leaving the projected jet structure collinear to $\sim 4°$ are unlikely to occur.

We have no convincing model to explain the origin of the kinematic asymmetry in 3C 171, but it is clear from even idealized simulations of jet hydrodynamics (Norman *et al.* 1982) that the kinematics of entrained material will be highly complex and time-dependent. Identification of observed gas velocities with any characteristic velocities in the radio plasma is risky business indeed.

5. *The radio sources are of low to moderate radio power.* 3C 171 is a glaring exception to this trend, since it has a very high radio luminosity ($\sim 10^{44}$ ergs s^{-1}). As described above, this is important for several reasons. First, it proves that the phenomenon of optical emission-line gas in radio lobes is not confined to low-luminosity radio sources. Even very high luminosity radio sources (and the highly energetic jets which feed them) appear capable of entraining cool, dense (optically emitting) gas. Second, the large radio luminosity of 3C 171 places very severe energetic constraints on an interpretation of the observed emission-line velocities as being those of the energy-carrying jet fluid (see above).

6. *The line-emitting gas is located at distances less than about 100 kiloparsecs from the galaxy nucleus.* 3C 171 is typical in this case, and we interpret this as being consistent with our hypothesis (e.g., van Breugel *et al.* 1984*a*) that the emission-line gas is preexisting galactic halo material which is lit up and accelerated by the radio plasma. This is because the dense gaseous medium necessary to produce the emission-line clouds is only likely to exist on galactic or circumgalactic scales.

7. *The spectrum of the emission-line gas in radio lobes strongly resembles the spectra of the narrow-line region in active galaxies.* The gas immersed in the radio plasma is presumably being ionized by processes which are similar to those occurring in the narrow-line region (photoionization by a hard continuum, or possibly collisional ionization by relativistic particles). The blue extranuclear continuum detected near the radio lobes/emission-line gas in 3C 171 is in fact suggestive of photoionization by an *in situ* source. Of equal significance for understanding the ionization source are the low gas temperatures we measure in the radio lobes ($\leq 2 \times 10^4$ K). These effectively rule out collisional ionization of the gas by shocks (e.g., Ferland and Netzer 1983).

We would like to thank the staffs of the Kitt Peak National Observatory and the National Radio Astronomy Observatory for the excellent support they provided during the data acquisition and reduction pertinent to this paper. We thank W. Keel and R. Laing for showing us their unpublished data on 3C 171. We also thank D. Eichler, A. Gower, R. Laing, and A. Wilson for informative conversations. T. M. H. and G. K. M. acknowledge the support of NATO research grant 1828, T. M. H. acknowledges the support of NSF grant AST-82-16553, and the support of the Alfred P. Sloan Foundation. T. M. H. also thanks the Laboratory for Astronomy and Solar Physics at NASA/Goddard Space Flight Center for support in the form of a NASA/ASEE Summer Faculty Fellowship.

REFERENCES

Balick, B., and Heckman, T. M. 1983, *Ap. J. (Letters)*, **265**, L1.
Bridle, A. H., and Perley, R. A. 1984, *Ann. Rev. Astr. Ap.*, **22**, in press.
Burbidge, G. R., and Crowne, A. H. 1979, *Ap. J. Suppl.*, **40**, 583.
De Young, D. 1981, *Nature*, **293**, 43.
———. 1982, in *IAU Symposium 97, Extragalactic Radio Sources*, ed. D. S. Heeschen and C. M. Wade (Dordrecht: Reidel), p. 69.
Fanaroff, B. L., and Riley, J. M. 1974, *M.N.R.A.S.*, **167**, 31P.
Ferland, G., and Netzer, H. 1983, *Ap. J.*, **264**, 105.
Graham, J. A. 1983, *Ap. J.*, **269**, 440.
Hardee, P. E., Eilek, J. A., and Owen, F. N. 1980, *Ap. J.*, **242**, 502.
Heckman, T. M. 1980, *Astr. Ap.*, **81**, 152.
Heckman, T. M., Miley, G. K., Balick, B., van Breugel, W. J. M., and Butcher, H. R. 1982, *Ap. J.*, **262**, 529.
Keel, W., and Miller, J. S. 1983, private communication.
Koski, A. T. 1978, *Ap. J.*, **223**, 56.
Kühr, H., Nauber, U., Pauliny-Toth, I. I. K., and Witzel, A. 1979, *A Catalog of Radio Sources* (Bonn: Max-Planck-Institut für Radio Astronomie).
Laing, R. A. 1981, *M.N.R.A.S.*, **195**, 261.
Laing, R. A., Riley, J. M., and Longair, M. S. 1983, *M.N.R.A.S.*, **204**, 151.
Miley, G. K. 1980, *Ann. Rev. Astr. Ap.*, **18**, 165.
———. 1983, Jet Workshop, Torino.
Miley, G. K., Heckman, T. M., Butcher, H. R., and van Breugel. W. J. M. 1981, *Ap. J. (Letters)*, **247**, L5.
Miller, J. S. 1981, *Pub. A.S.P.*, **93**, 681.
Norman, M. L., Smarr, L., Winkler, K. H. A., and Smith, M. D. 1982, *Astr. Ap.*, **113**, 285.
Osterbrock, D. E. 1974, *Astrophysics of Gaseous Nebulae* (San Francisco: W. H. Freeman).
Owen, F., and Rudnick, L. 1976, *Ap. J. (Letters)*, **205**, L1.
Simard-Normandin, M., Kronberg, P. P., and Button, S. 1981, *Ap. J. Suppl.*, **45**, 97.
van Breugel, W. J. M., and Heckman, T. M. 1982, in *IAU Symposium 97, Extragalactic Radio Sources*, ed. D. S. Heeschen and C. M. Wade (Dordrecht: Reidel), 71.
van Breugel, W. J. M., Heckman, T. M., and Miley, G. K. 1984*a*, *Ap. J.*, **276**, 79.
———. 1984*b*, in preparation.
van Breugel, W.J.M., Miley, G.K., Heckman, T.M., Butcher, H.R., and Bridle, A. 1984, *Ap. J.*, submitted.
Yee, H. K. C., and Oke, J. B. 1978, *Ap. J.*, **226**, 753.

T. M. HECKMAN: Astronomy Program, University of Maryland, College Park, MD 20742
G. K. MILEY: Sterrewacht Leiden, Postbus 9513, 2300 RA Leiden, The Netherlands
W. J. M. VAN BREUGEL: Dept. of Astronomy, University of California, Berkeley, CA 94720

PLATE 18

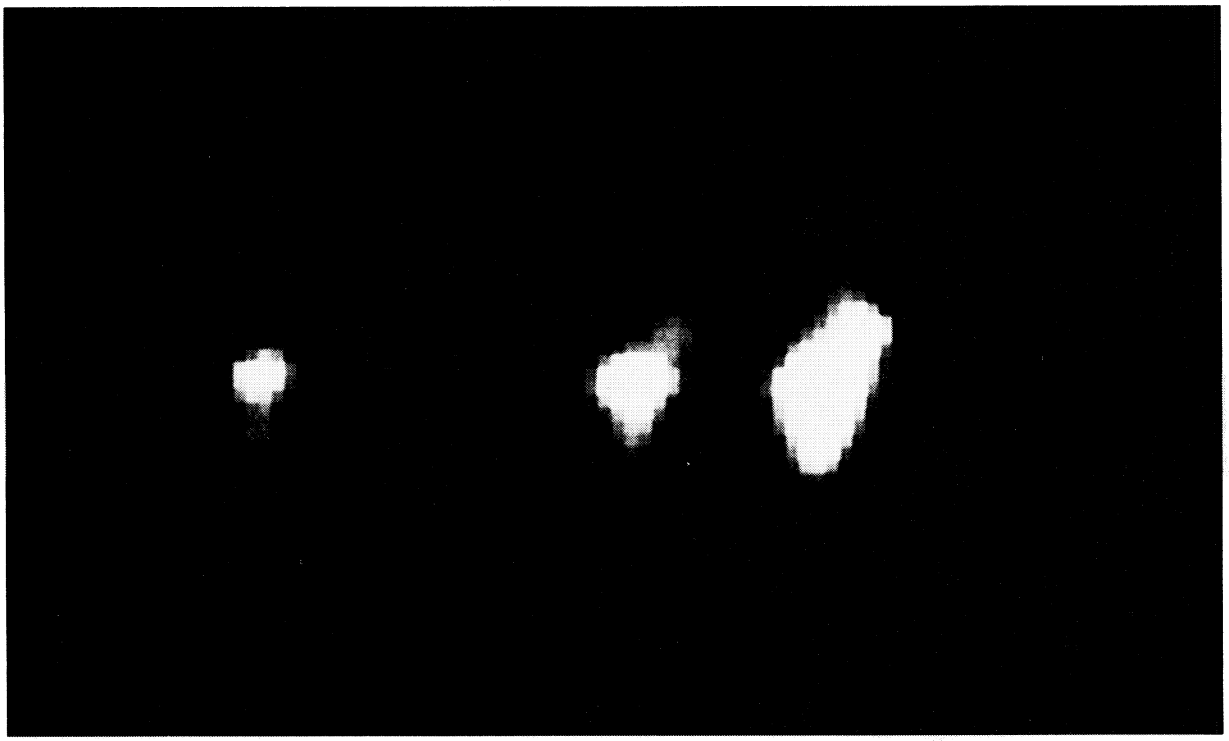

FIG. 1.—Gray-scale representation of the long-slit Cryogenic Camera spectroscopic data in P.A. = 102° (along the radio axis). Wavelength increases to the right, and west is to the top. The displayed region is 46″ long in P.A. = 102°. The three spatially extended emission lines are Hβ and [O III] λ4959 and λ5007.

HECKMAN, VAN BREUGEL, AND MILEY (*see* page 510)

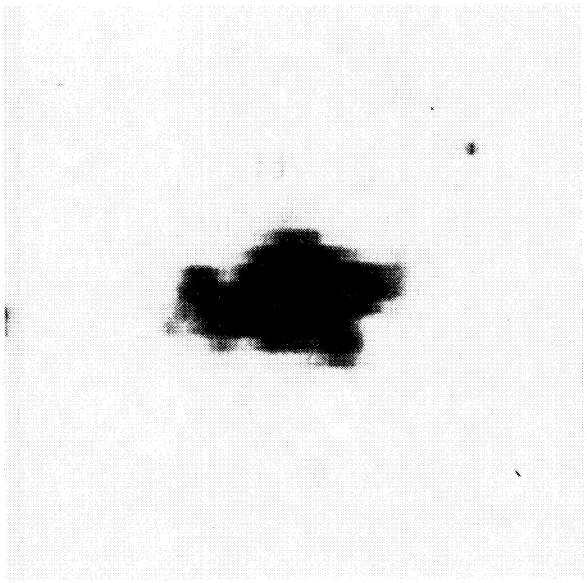

FIG. 2.—Gray-scale representation of the Prime Focus CCD *R* band image of 3C 171. The portion of the image which is displayed is 23″ square with east to the left and north to the top. The material protruding E/W from 3C 171 is emission-line gas (imaged in redshifted Hβ and [O III] $\lambda\lambda$4959, 5007).

HECKMAN, VAN BREUGEL, AND MILEY (*see* page 510)